

Nanoscale

Accepted Manuscript



This is an *Accepted Manuscript*, which has been through the Royal Society of Chemistry peer review process and has been accepted for publication.

Accepted Manuscripts are published online shortly after acceptance, before technical editing, formatting and proof reading. Using this free service, authors can make their results available to the community, in citable form, before we publish the edited article. We will replace this *Accepted Manuscript* with the edited and formatted *Advance Article* as soon as it is available.

You can find more information about *Accepted Manuscripts* in the [Information for Authors](#).

Please note that technical editing may introduce minor changes to the text and/or graphics, which may alter content. The journal's standard [Terms & Conditions](#) and the [Ethical guidelines](#) still apply. In no event shall the Royal Society of Chemistry be held responsible for any errors or omissions in this *Accepted Manuscript* or any consequences arising from the use of any information it contains.

ARTICLE

Reduced Graphene Oxide Growth on 316L Stainless Steel for Medical Applications.

Cite this: DOI: 10.1039/x0xx00000x

L. Cardenas^{*ab}, J. MacLeod^a, J. Lipton-Duffin^a, D.G Seifu^b, F. Popescu^c, M. Sijac^c, D. Mantovani^b, F. Rosei^{*ad}

Received 00th 2014,
Accepted 00th 2014

DOI: 10.1039/x0xx00000x

www.rsc.org/

We report a new method for the growth of reduced graphene oxide (rGO) on the 316L alloy of stainless steel (SS) and its relevance for biomedical applications. We demonstrate that electrochemical etching increases the concentration of metallic species on the surface and enables the growth of rGO. This result is supported through a combination of Raman spectroscopy, X-ray photoelectron spectroscopy (XPS), atomic force microscopy (AFM), scanning electron microscopy (SEM), density functional theory (DFT) calculations and static water contact angle measurements. Raman spectroscopy identifies the G and D bands for oxidized species of graphene at 1595 cm⁻¹ and 1350 cm⁻¹, respectively, and gives an I_D/I_G ratio of 1.2, indicating a moderate degree of oxidation. XPS shows -OH and -COOH groups in the rGO stoichiometry and static contact angle measurements confirm the wettability of rGO. SEM and AFM measurements were performed on different substrates before and after coronene treatment to confirm rGO growth. Cell viability studies carried out using mammalian cells reveal that these rGO coatings do not have toxic effects on mammalian cells, making this material suitable for biomedical and biotechnological applications.

Introduction

The fabrication of implantable devices exhibiting superior corrosion and high mechanical resistance properties has been the focus of extensive efforts during the past decades.^{1,2} Stainless steel 316L (SS316L) is one of the most commonly used materials for the fabrication of implantable devices. SS316L is used extensively in coronary/cardiovascular stents,^{3,4} cranial fixation,⁵ orthopedic stents^{6,7} and dental implants.^{8,9} However, it exhibits limited resistance to corrosion and wear, which can lead to degradation of the material and its subsequent release of potential harmful metallic ions, thereby contributing to clinical complications such as thrombus and apoptosis.¹⁰ Although SS316L is natively covered with a passivating layer of metal oxides, this is not sufficient to protect it against localized forms of corrosion (pitting) associated with chloride ions in aqueous environments.¹¹ The human body is not a friendly environment for implanted materials, mostly due to the presence of highly oxygenated saline electrolyte, which can cause the corrosion and subsequent degradation of SS316L.¹² In addition, physiological conditions exert pressure/friction against the surface of medical devices, requiring high mechanical resistance to wear.

Coating SS316L with a protective layer can improve its mechanical and anticorrosive properties. Graphene (Gr) and related materials could be excellent candidates as protective coatings, since they exhibit extraordinary mechanical¹³ and anticorrosion¹⁴ properties. Stiffness and strength are the key factors in determining the stability and lifetime of medical

devices. Gr is one of the strongest known materials, possessing an ultrahigh Young's modulus of ~1 TPa and an intrinsic fracture strength of ~130 GPa.¹³ Extensive efforts have been devoted to the study of the effects of growing or attaching Gr layers over corrosion-prone surfaces, such as copper and nickel. These studies have demonstrated that Gr coatings grown by chemical vapour deposition provide significant corrosion protection as compared to the bare metallic substrates.^{14,15} More recently, other studies suggest that Gr is an effective oxidation inhibitor on copper,^{16,17} and silicon,¹⁷ albeit over short time scales only (ca. 1 month). Gr coatings inhibit oxidation because they are impermeable to all standard gases.¹⁸ These mechanical and anticorrosive properties make Gr an excellent candidate for the fabrication of protective layers on SS316L for implantable devices.

In addition to having excellent physical and chemical properties, Gr is also gathering interest in the biomedical field,¹⁹ where it is used as a new component in biosensors,²⁰⁻²¹ tissue engineering^{22,23} and drug delivery.^{24,25} Most biological tests, including biological response and safety tests, have been conducted on reduced Gr oxide (rGO) and Gr oxide (GO). This is because rGO and GO are more hydrophilic than pristine Gr. This hydrophilicity renders rGO and GO soluble in water and allows them to remain stably dispersed,²⁶ thus improving their potential to act as surface coatings with improved biocompatibility. Coating SS316L with an oxidized form of Gr could produce a material useful for a broad range of biomedical applications, especially when considering the possibility of

controlling its properties such as available reactive oxygen species, surface area, cytotoxicity and corrosion resistance. Here, we present a new method for synthesizing rGO directly on SS316L.²⁷ Our approach is scalable and produces rGO coatings that foster good cell viability and stability.

Materials and methods

Electropolishing of SS 316L. Single-side mirror polished SS316L foils (Goodfellow Cambridge Limited, thickness 0.9 mm) were used as the anode of an electrochemical cell, while a copper plate was used as cathode. The electrolyte solution was a mixture of 8 parts by volume of orthophosphoric acid (85%, Fisher Scientific), 2 parts distilled deionized water, and 1 part sulphuric acid (98%, ReAgent supplies). The voltage was kept constant at 3.8 V, with a current density of 5×10^{-3} mA/mm², with a total electropolishing time of 5 min. Following electropolishing, the SS316L foil was cleaned by sonication in ethanol.

Preparation of rGO coating. Coronene (97%, Sigma Aldrich) was dissolved in trichlorobenzene (TCB, 99%, Sigma-Aldrich) at a concentration between 10^{-4} and 10^{-5} M. The coronene solution was drop cast onto electropolished SS316L. Samples were heated between 600 °C and 800 °C for 30 minutes under a flowing atmosphere of 98% nitrogen and 2% hydrogen in a quartz tube.²⁸ After annealing, the furnace was cooled over 10 min while maintaining the N₂/H₂ flow.

Characterization methods. Raman spectroscopy was performed in the region of 800–3500 cm⁻¹ using an inVia Raman microscope (Renishaw with a laser wavelength of 514 nm). Scanning with this instrument was used to evaluate the presence and uniformity of rGO on the SS316L. X-ray photoelectron spectroscopy (XPS) was performed using a Mg K_α source in a commercial instrument (VG ESCALAB 220i XL), and revealed well-resolved peaks corresponding to C1s, O1s, Ni2p, Cr2p, Fe2p. Each high-resolution spectrum was decomposed into a combination of Voigt functions, each with an overall full-width at half maximum (FWHM) of approximately 1.4 eV. ScanAsyst mode atomic force microscopy (AFM) using an Agilent 5500 microscope was employed to study in situ the changes of the sample surfaces before and after rGO growth. Topography images are recorded in ScanAsyst mapping mode using Si cantilevers with a spring constant of 0.2 N/m and typical radius of about 20–25 nm. AFM topography images were analyzed using WSxM software.²⁹ Static contact angle measurements were carried out using a homemade injection system; 10 μL of deionized water was deposited on rGO through a 160 μm diameter capillary. The images were analyzed and treated using the ImageJ software³⁰ with the LBADSA plugin.³¹

Ab initio calculations. Density functional theory (DFT) calculations were carried out to identify the vibrational frequencies and Raman intensities for the coronene monomer, dimer and trimer configurations. Calculations were performed using Gaussian 09³² by DFT at the B3LYP level³³ using the 6-31G basis set.

Cell toxicity experiments. The different samples were placed in six-well culture plates (SARSTEDT Inc. Newton, NC, USA). After fixing the samples in the well they were sterilized using 70% ethanol, washed with 1X phosphate buffered saline (1XPBS) twice, UV was applied for 2 h on both sides and finally they were again washed with 1XPBS twice. Subsequently the samples were incubated at 4 °C overnight

with 1 ml culture medium on a shaker. At the same time 2.5×10^4 human umbilical vein endothelial cells (HUVECs) were seeded on 96-wall tissue culture plate (SARSTEDT Inc. Newton, NC, USA) and the cells were allowed to grow for 24 h. Afterwards the medium was replaced by the medium incubated 24 h with the samples and cells were further allowed to grow for 24 h. Finally, the cellular viability was quantified using resazurin as a redox indicator. Resazurin (7-hydroxy-3H-phenoxazin-3-one 10-oxide) is a fluorescent common dye marker used as an indicator for cell viability in HUVEC cultures. Resazurin fluoresces and changes color in response to the chemical reduction of the culture medium, resulting from cell growth. In this process the resazurin^{34,35} is irreversibly reduced to resorufin.³⁵

Results and discussion

XPS reveals that electrochemical polishing of bare SS316L enriches the surface content of metallic nickel, iron and chromium. Spectra are shown in Fig. 1 for the Ni 2p_{3/2}, Fe 2p_{3/2} and Cr 2p_{3/2} core levels for unpolished SS316L polished SS 316L samples. The surface of the untreated sample has no detectable nickel, nor any metallic states of iron or chromium at the surface. However, the spectra for treated SS316L reveal a significant nickel concentration (9.4%) at the surface, with two well-resolved contributions and a shoulder. These features may be assigned as metallic nickel (853.2 eV), and nickel (II) oxide (856.6 eV). Likewise, iron and chromium increase in concentration at the surface to 42.4% and 48.0% respectively, including metallic states corresponding to Fe(0) at 707 eV and Cr(0) at 573 eV.

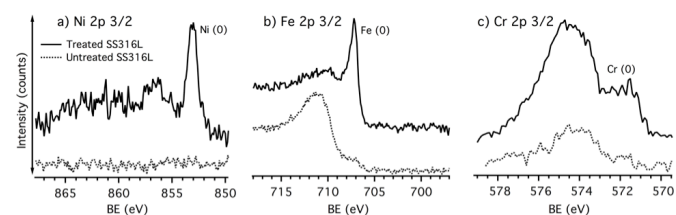
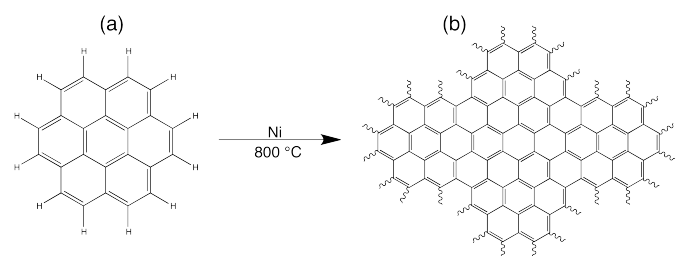


Figure 1. XPS spectra of Ni 2p_{3/2}, Fe 2p_{3/2}, Cr 2p_{3/2} for untreated SS 316L (below) and treated SS 316L (above).

Coronene was applied dropwise from solution to the SS samples, which were subsequently annealed at 800 °C for 30 minutes (see materials and methods).³⁶ Coronene was chosen as the precursor based on its relatively high thermo-resistivity: dimerization happens in powder samples between 550 °C and 600 °C.³⁷ From a structural point of view, coronene is essentially a small flake of graphene, comprising sp₂ carbon formed by six cyclobenzenes (Scheme 1).



Scheme 1. (a) Molecular model of coronene. (b) Subsequent polymerization of coronene by dehydrogenation and rebonding.

Raman spectroscopy has been widely used on carbonaceous systems such as carbon nanotubes,³⁸ fullerenes,³⁹ and graphene.^{40,41} This powerful technique makes it possible to obtain spectroscopic signatures of hybridized carbon sp_2 bonds present in honeycomb networks. Raman spectra exhibit characteristic bands for these materials; among them are the G line at ca. 1585 cm^{-1} and the D band around 1350 cm^{-1} .⁴⁰⁻⁴² The G band describes a stretching mode attributable to sp_2 -hybridized carbon atoms in the honeycomb network.⁴³ The D band characterizes disordered and amorphous carbon bonds and originates from the breathing mode of k -point phonons of A_1 symmetry.⁴² At high wavenumbers a series of overtones from both D and G are visible between ca. 2700 and 3300 cm^{-1} .⁴³

The Raman spectrum of pristine coronene supported on glass (Fig 2a, blue curve) shows a strong D band at 1359 cm^{-1} , with a small G line at 1600 cm^{-1} . The intensity amplitude ratio I_D/I_G is 7.88, consistent with the relatively small spatial extent of the sp_2 network in coronene. The Raman spectrum for the annealed coronene film on untreated SS316L (Fig 2a, black curve) has a broader and more intense D band at 1359 cm^{-1} . The G band at 1597 cm^{-1} is virtually non-existent. This suggests that graphene does not grow on the untreated SS316L surface. In the case of the annealed coronene film on treated SS316L (Fig 2a, red curve) the Raman spectrum exhibits broader and more intense peaks. The G band is shifted to 1597 cm^{-1} whereas the D band appears at 1359 cm^{-1} , in agreement with earlier reports of rGO.⁴⁴ The average size of sp_2 -bonded graphitic domains is inversely proportional to the I_D/I_G ratio;⁴⁵ the ratio I_D/I_G from our samples is approximately 1.2, which is also consistent with ratios reported for other rGO materials.⁴⁵ This indicates that the sp_2 network extends much further than it does in the coronene molecule, a clear signature of oligomerization and expansion of the graphene lattice. These results are consistent with the formation of rGO on the treated SS316L surface.

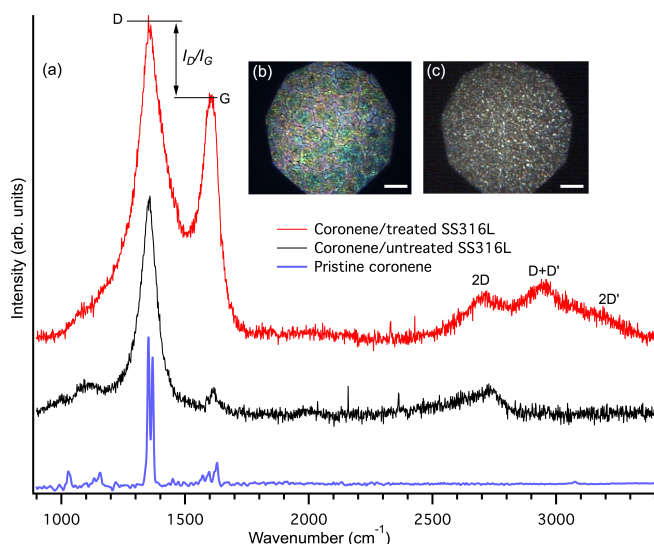


Figure 2. (a) Raman spectra corresponding to rGO (red curve), coronene on untreated SS316L (black curve) and coronene on glass (blue curve) on the same area where optical images were taken for: (b) rGO/SS 316L and (c) coronene/untreated SS316L. Scale bars in the inset images represent $20\text{ }\mu\text{m}$.

Figures 2b and 2c display optical microscopy images of the rGO (coronene/treated SS316L) and the coronene/untreated SS316L samples in the region where the Raman spectra were acquired. Two important features are discernible in the image of the treated sample (Fig. 2b): i) a colour variation due to the intrinsic reflectance of graphene oxide;⁴⁶ and ii) graphene-like 120° grain boundaries, consistent with previous observations.⁴⁷ These features are absent in the image of coronene/untreated SS316L (Fig. 2c).

AFM was used to inspect the surface morphology of untreated SS316L, treated SS316L and rGO/SS316L. Untreated SS316L (Figure 3a) presents patterns of well-defined grain boundaries characteristic of stainless steel.⁴⁸ After treatment (Figure 3b) the surface becomes considerably smoother. Following the rGO coating, the steel surface becomes populated with multi-layered arrangements of flakes as seen in the AFM image displayed in Figure 3c. The heights of layered rGO platelets follow a roughly normal distribution with a mean height of $23\pm 2\text{ nm}$ and a standard deviation of $9\pm 2\text{ nm}$. A clearer illustration of the rGO/SS316L surface is given by the SEM image in Figure 3d. Flakes completely cover the surface and follow its contour.

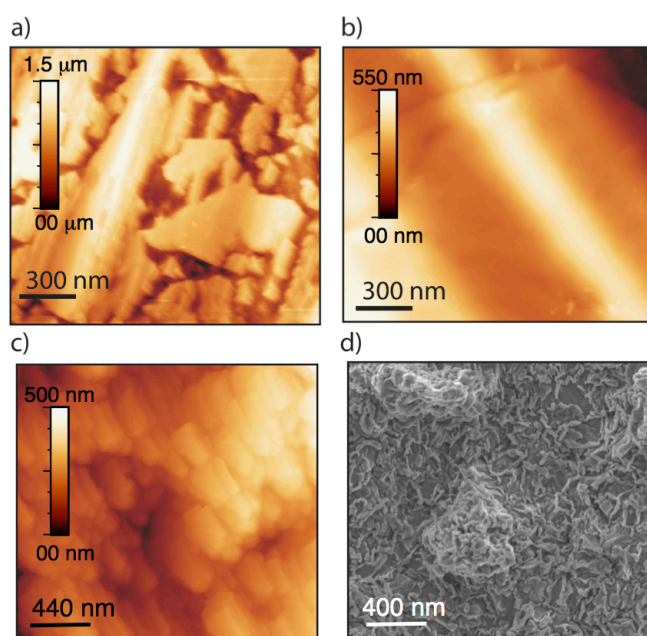


Figure 3. AFM images on untreated SS316L (a), treated SS316L (b) and rGO/SS316L (c). SEM image on rGO/SS316L (d).

DFT at the B3LYP level³³ was used to investigate the theoretical Raman spectra of successive oligomerizations of coronene, in monomer (Fig. 4a, red curve), trimer (Fig. 4a, black curve) and tetramer (Fig. 4a, blue curve) configurations.[§] The calculated Raman spectrum (Fig. 4a) for a single coronene molecule has D and G bands at ca. 1407 cm^{-1} and ca. 1656 cm^{-1} respectively, yielding an I_D/I_G ratio of ~ 3 . Figure 4b shows the decreasing evolution of the I_D/I_G ratio for successively larger oligomers, consistent with the spatial expansion of the network of sp_2 -graphitic bonds.

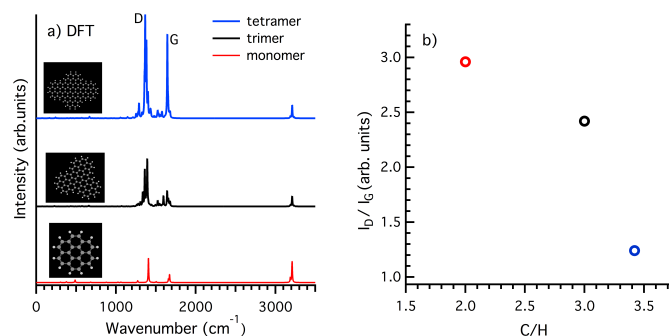


Figure 4. (a) Calculated Raman spectra for each DFT optimized structures (single-coronene, trimer-coronene and tetramer-coronene). (b) Carbon – Hydrogen (C/H) vs ID/IG ratios.

Figure 5 shows XPS spectra of the C1s and O1s core levels were obtained from the rGO/SS316L, treated SS316L and untreated SS316L samples. The C1s peak (bottom, Fig. 5a) on untreated/SS316L is broad, with a shoulder at high binding energy. The contribution located at 284.9 eV is attributable to C(sp₃) bonds. The shoulder can be fit with by three contributions, one corresponding to COH groups (pink curve, 286.6 eV), one attributable to CO (light blue curve, 288.1) and the last to –COOH groups (violet curve, 289.0 eV) with a concentration of 2.9%. After treatment, the concentration of COH groups increases significantly and –COOH decreases to a relative concentration of 0.5% (middle, Fig. 5a). Growing rGO on the treated surface reveals a new contribution at 284.3 eV corresponding to C(sp₂) bonds accompanied by the increase of the –COOH contribution (relative concentration, 4.1 %). Figure 5b shows core level spectra of O1s for rGO/SS316L, treated and untreated SS316L, which can be fit by three peaks attributable to O²⁻, hydroxyl groups (OH⁻) and hydrate or water (OH₂). The O²⁻ contribution is associated with metallic oxide states on the surface (relative concentration, 33.1%). The O1s core levels reveal the crucial importance of electrochemical etching through to a pronounced decrease of this contribution (concentration, 18.0%). The top spectrum, of SS with rGO, exhibits a recovered intensity of this O²⁻ contribution with a concentration of 22.5%.

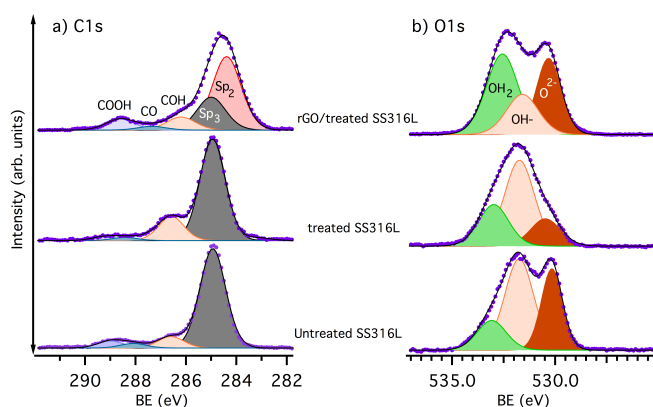


Figure 5. XPS spectra of (a) C1s, and (b) O1s on untreated SS316L, treated SS316L and rGO/SS.

The presence of hydroxyl groups on the rGO is confirmed by both the C1s and O1s spectra. These XPS data are consistent with the Lerf and Klinowski model for GO, in which carboxylic

acid groups are primarily located on the periphery of the basal plane of platelets of GO, whereas hydroxyl groups are incorporated in the graphene structure⁴⁹. An analysis of the XPS signals shows that these functional groups (–OH– or –COOH) cover about 18% of the surface respect to 10% expected for rGO.⁵⁰

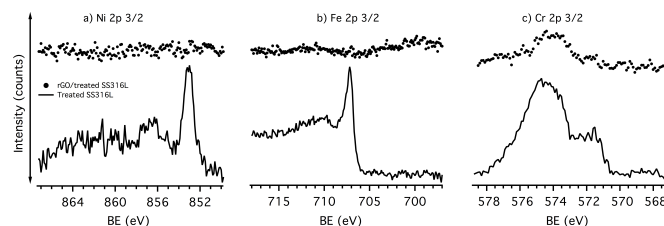


Figure 6. XPS spectra of Ni 2p_{3/2}, Fe 2p_{3/2}, Cr 2p_{3/2} for treated SS316L (below) and rGO/treated SS316L (above).

Carbon-metal bonds were not detected in the C1s core level spectrum. In addition, Ni2p and Fe2p core level did not appear in the XPS spectra (Fig. 6a and 6b) after rGO growth. This indicates that these metallic elements, which are of course present in the SS, are buried by the rGO layer and are immiscible. This is an important aspect in relation to biological applications. However, a small amount of oxidized Cr2p was observed on the rGO/treated SS316L sample (Fig. 6c). This signal (Cr2p) is consistent with the higher initial concentration of chromium (48%) in treated SS316L, which is visible even after graphene growth on the treated SS316L sample. It has recently been suggested that the presence of metallic chromium on the surface may be detrimental to graphene growth under certain conditions.⁵¹ Our results here show that the presence of chromium oxide does not preclude the growth of the graphene oxide.

The wettability of the rGO layers, along with untreated and treated SS 316L samples, was tested by measuring static water contact angles (Fig. 7). The mean static contact angle between rGO/treated SS316L and water was found to be 62°±2° (Fig. 7c). Untreated and treated SS316L were used as references, with mean contact angles of 92°±2° (Fig. 7a) and 52°±2° (Fig. 7b), respectively. The difference between the static water contact angles on untreated and treated SS316L is due to the addition of water molecules to SS316L. This effect, known as hydrolysis, is induced by electrochemical etching.¹¹ These measurements confirm that the rGO layer improves the SS316L wettability due to its hydroxyl and carboxylic groups, as confirmed by our previous XPS analysis on rGO/SS.



Figure 7. Water droplet on untreated SS316L (a), treated SS316L (b), and rGO/treated SS316L (c), showing a schematic angle measurement (white lines).

Cell viability of rGO. Cytotoxicity tests were carried out on rGO, treated SS and untreated SS. Human Umbilical Vein Endothelial Cells (HUVECs) growth was used to quantify the cytotoxicity of each sample. HUVECs are sensitive compared to fibroblast and smooth muscle cells, and are the cells that line the inner surface of blood vessels,⁵² therefore, they are an extremely pertinent model for testing the cytotoxicity of the rGO/SS316L for vascular and cardiac stent applications.

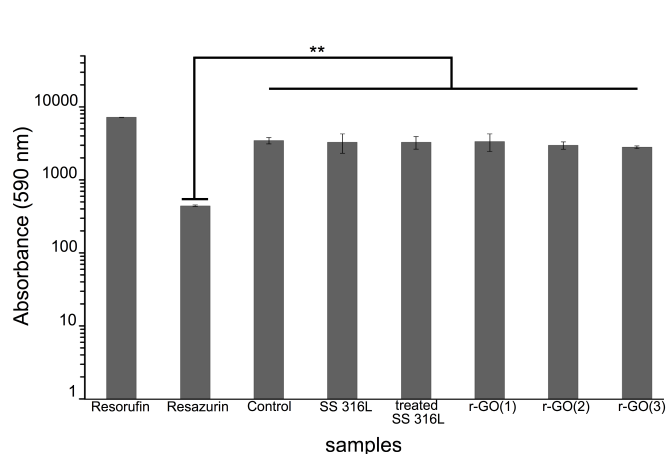


Figure 8. HUVEC cell viability after exposure to untreated SS 316L, treated SS 316L and rGO (triple sampling for repeated surveys) based on the Alamar blue assay. Fluorescence signals are proportional to the number and metabolic activity of the cells. Statistical analysis was performed using a Student's *t*-test ($p < 0.05$).

The Alamar blue assay for HUVECs quantification is a common method for screening the adverse effect of nanomaterials in cell culture.⁵³ The Alamar blue assay test was performed after 48 h of incubation. The medium was removed from the culture dishes and the adhered cells were washed twice with 1X phosphate buffered saline (1XPBS) and new cell culture media was added to the culture dishes. Afterwards Alamar blue was added directly into the culture medium at a final concentration of 10%. The fluorescence was measured at 540 nm excitation wavelength and 590 nm emission wavelength using a microplate spectrometer (FL600 Microplate Fluorescence Reader, BIO-TEK, Winooski VT, USA). Alamar blue solution was also added to a medium without cells, as a negative control. An Alamar blue containing culture dish with a confluent layer of HUVECs served as a positive control in addition to that pure Resorufin absorbance was measured. The measured fluorescence signals are proportional to the number and metabolic activity of the cells. Statistical analysis was performed using the Student's *t*-test ($p < 0.05$) (see Fig. 8).

The phase-contrast microscopy images (2D cultures) presented in Figure 9 demonstrate that the morphology and spreading of cells were not affected compared to the control for all the three samples (rGO, untreated SS and treated SS). The Alamar blue absorbance data presented in Figure 8 confirmed that none of the samples were toxic to HUVECs. There is no significant difference in the absorbance of resorufin between the control and the three different samples. Our data demonstrate excellent cell viability when tested with non-contact toxicity for all samples, and indicate that none of the treated samples leached any toxic species into the culture medium when following standard sterilization procedures.

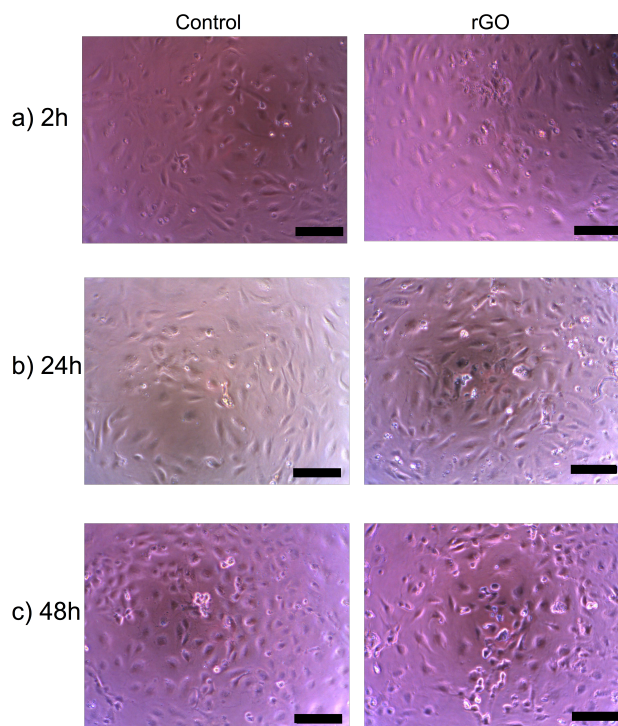


Figure 9. Phase-contrast microscopy images of cells grown on the control (left) and rGO (right) samples, respectively incubated for: (a) 2h, (b) 24h and (c) 48h. Scale bars in the inset images represent 100 μm .

Conclusions

We developed a method for producing a rGO coating on SS316L. The rGO coating was synthesized from coronene by solution deposition and subsequent annealing. Although SS316L is not a known platform for catalytic growth of graphene-like material, we demonstrated that electrochemical etching increases the free metal concentration on the surface and allows rGO growth. Cytotoxicity studies demonstrate that rGO/SS316L does not have toxic effects on mammalian cells. rGO coatings could significantly improve the mechanical and biological properties, improving the properties of stainless steel for biomedical and biotechnology applications.

Acknowledgements

F.R. and D.M. acknowledge partial salary support from the Canada Research Chairs program. L.C. acknowledges partial salary support through a personal fellowship from FRSQ. F.R. and D.M. are supported through individual Discovery Grants from NSERC. F.R. is grateful to NSERC for an EWR Steacie Memorial Fellowship. We acknowledge funding from FRQNT through a team grant. This research has been enabled by the use of computing resources provided by WestGrid and Compute/Calcul Canada. We thank Mr. C. Chabanier for help with contact angle measurements.

Notes and references

^a INRS -Centre Énergie, Matériaux et Télécommunications, Boulevard Lionel-Boulet, Varennes, Québec, J3X 1S2, Canada. E-mail: luis.cardenas@ircelyon.univ-lyon1.fr; rosei@emt.inrs.ca

- ^b Laboratory for Biomaterials and Bioengineering, CRC-I, Department of Mining, Metallurgical and Materials Engineering & Research Center of CHU de Québec, Laval University, Québec City, QC, G1V 0A6, Canada.
- ^c Département de Chimie et Biochimie, Université du Québec à Montréal, Montréal, QC H3C 3P8, Canada.
- ^d Center for Self-Assembled Chemical Structures, McGill University, H3A 2K6 Montreal, Quebec, Canada.
- § Note that dimer, trimer and tetramer configurations of coronene are a chemical structure formed from two, three and four identical sub-units of coronene.
- D. F. Williams, *Biomaterials*, 2008, **29**, 2941–53.
 - F. Variola, F. Vetrone, L. Richert, P. Jedrzejowski, J.-H. Yi, S. Zalzal, S. Clair, A. Sarkissian, D. F. Perepichka, J. D. Wuest, F. Rosei, and A. Nanci, *Small*, 2009, **5**, 996–1006.
 - F. Airoidi, A. Colombo, D. Tavano, G. Stankovic, S. Klugmann, V. Paolillo, E. Bonizzoni, C. Briguori, M. Carlino, M. Montorfano, F. Liistro, A. Castelli, A. Ferrari, F. Sgura, and C. Di Mario, *Am. J. Cardiol.*, 2004, **93**, 474–7.
 - C. Bayram, A. K. Mizrak, S. Aktürk, H. Kursaklioglu, A. Iyiso, A. Ifran, and E. B. Denkbaş, *Biomed. Mater.*, 2010, **5**, 055007.
 - W. C. Broaddus, K. L. Holloway, C. J. Winters, M. R. Bullock, R. S. Graham, B. E. Mathern, J. D. Ward, and H. F. Young, *J. Neurosurg.*, 2002, **96**, 244–7.
 - L. Reclaru, R. Lerf, P. Y. Eschler, and J. M. Meyer, *Biomaterials*, 2001, **22**, 269–79.
 - C. N. Kraft, B. Burian, L. Perlick, M. A. Wimmer, T. Wallny, O. Schmitt, and O. Diedrich, *J. Biomed. Mater. Res.*, 2001, **57**, 404–12.
 - P. Neumann, C. Bourauel, and A. Jäger, *J. Mater. Sci. Mater. Med.*, 2002, **13**, 141–7.
 - Y. Yonekura, K. Endo, M. Iijima, H. Ohno, and I. Mizoguchi, *Dent. Mater. J.*, 2004, **23**, 197–202.
 - O. F. Bertrand, R. Sipehia, R. Mongrain, J. Rodés, J. C. Tardif, L. Bilodeau, G. Côté, and M. G. Bourassa, *J. Am. Coll. Cardiol.*, 1998, **32**, 562–71.
 - M. P. Ryan, D. E. Williams, R. J. Chater, B. M. Hutton, and D. S. McPhail, *Nature*, 2002, **415**, 770–4.
 - K. Hashimoto, M. Seo, G. Herting, I. Odnevall Wallinder, and C. Leygraf, *Corros. Sci.*, 2007, **49**, 103–111.
 - C. Lee, X. Wei, J. W. Kysar, and J. Hone, *Science*, 2008, **321**, 385–8.
 - S. Chen, L. Brown, M. Levendorf, W. Cai, S.-Y. Ju, J. Edgeworth, X. Li, C. W. Magnuson, A. Velamakanni, R. D. Piner, J. Kang, J. Park, and R. S. Ruoff, *ACS Nano*, 2011, **5**, 1321–7.
 - D. Prasai, J. C. Tuberquia, R. R. Harl, G. K. Jennings, B. R. Rogers, and K. I. Bolotin, *ACS Nano*, 2012, **6**, 1102–8.
 - F. Zhou, Z. Li, G. J. Shenoy, L. Li, and H. Liu, *ACS Nano*, 2013, **7**, 6939–6947.
 - M. Schriver, W. Regan, W. J. Gannett, A. M. Zaniewski, M. F. Crommie, and A. Zettl, *ACS Nano*, 2013, **7**, 5763–8.
 - J. S. Bunch, S. S. Verbridge, J. S. Alden, A. M. van der Zande, J. M. Parpia, H. G. Craighead, and P. L. McEuen, *Nano Lett.*, 2008, **8**, 2458–62.
 - Y. Zhang, T. R. Nayak, H. Hong, and W. Cai, *Nanoscale*, 2012, **4**, 3833–42.
 - K. P. Loh, Q. Bao, G. Eda, and M. Chhowalla, *Nat. Chem.*, 2010, **2**, 1015–24.
 - L. A. L. Tang, J. Wang, and K. P. Loh, *J. Am. Chem. Soc.*, 2010, **132**, 10976–7.
 - A. Sahu, W. Il Choi, and G. Tae, *Chem. Commun. (Camb.)*, 2012, **48**, 5820–2.
 - Y. Wang, W. C. Lee, K. K. Manga, P. K. Ang, J. Lu, Y. P. Liu, C. T. Lim, and K. P. Loh, *Adv. Mater.*, 2012, **24**, 4285–90.
 - Z. Liu, J. T. Robinson, X. Sun, and H. Dai, *J. Am. Chem. Soc.*, 2008, **130**, 10876–7.
 - X. Yang, N. Zhao, and F.-J. Xu, *Nanoscale*, 2014.
 - A. Bianco, *Angew. Chem. Int. Ed. Engl.*, 2013, **52**, 4986–97.
 - L. Cardenas, J. McLeod, J. Lipton-Duffin, and F. Rosei, *submitted to the U.S. Patent office. 61/896,278*, United States.
 - I. Vlasiouk, M. Regmi, P. Fulvio, S. Dai, P. Datskos, G. Eres, and S. Smirnov, *ACS Nano*, 2011, **5**, 6069–76.
 - I. Horcas, R. Fernández, J. M. Gómez-Rodríguez, J. Colchero, J. Gómez-Herrero, and A. M. Baro, *Rev. Sci. Instrum.*, 2007, **78**, 013705.
 - C. A. Schneider, W. S. Rasband, and K. W. Eliceiri, *Nat. Methods*, 2012, **9**, 671–675.
 - A. F. Stalder, G. Kulik, D. Sage, L. Barbieri, and P. Hoffmann, *Colloids Surfaces A Physicochem. Eng. Asp.*, 2006, **286**, 92–103.
 - M. J. Frisch, G. W. Trucks, H. B. Schlegel, G. E. Scuseria, M. A. Robb, J. R. Cheeseman, G. Scalmani, V. Barone, B. Mennucci, G. A. Petersson, H. Nakatsuji, M. Caricato, X. Li, H. P. Hratchian, A. F. Izmaylov, J. Bloino, G. Zheng, J. L. Sonnenberg, M. Hada, M. Ehara, K. Toyota, R. Fukuda, J. Hasegawa, M. Ishida, T. Nakajima, Y. Honda, O. Kitao, H. Nakai, T. Vreven, J. A. Montgomery, J. E. Peralta, F. Ogliaro, M. Bearpark, J. J. Heyd, E. Brothers, K. N. Kudin, V. N. Staroverov, R. Kobayashi, J. Normand, K. Raghavachari, A. Rendell, J. C. Burant, S. S. Iyengar, J. Tomasi, M. Cossi, N. Rega, J. M. Millam, M. Klene, J. E. Knox, J. B. Cross, V. Bakken, C. Adamo, J. Jaramillo, R. Gomperts, R. E. Stratmann, O. Yazyev, A. J. Austin, R. Cammi, C. Pomelli, J. W. Ochterski, R. L. Martin, K. Morokuma, V. G. Zakrzewski, G. A.

- Voth, P. Salvador, J. J. Dannenberg, S. Dapprich, A. D. Daniels, Ö. Farkas, J. B. Foresman, J. V. Ortiz, J. Cioslowski, and D. J. Fox, *Gaussian 09, Revision B.01*, Gaussian Inc. Wallingford CT 2009.
33. A. D. Becke, *J. Chem. Phys.*, 1993, **98**, 5648.
34. S. Anoopkumar-Dukie, J. B. Carey, T. Conere, E. O'sullivan, F. N. van Pelt, and A. Allshire, *Br. J. Radiol.*, 2005, **78**, 945–7.
35. J. O'Brien, I. Wilson, T. Orton, and F. Pognan, *Eur. J. Biochem.*, 2000, **267**, 5421–5426.
36. X. Wan, K. Chen, D. Liu, J. Chen, Q. Miao, and J. Xu, *Chem. Mater.*, 2012, **24**, 3906–3915.
37. A. V. Talyzin, S. M. Luzan, K. Leifer, S. Akhtar, J. Fetzer, F. Cataldo, Y. O. Tsybin, C. W. Tai, A. Dzwilewski, and E. Moons, *J. Phys. Chem. C*, 2011, **115**, 13207–13214.
38. M. S. Dresselhaus, A. Jorio, M. Hofmann, G. Dresselhaus, and R. Saito, *Nano Lett.*, 2010, **10**, 751–8.
39. H. Kuzmany, M. Matus, B. Burger, and J. Winter, *Adv. Mater.*, 1994, **6**, 731–745.
40. K. N. Kudin, B. Ozbas, H. C. Schniepp, R. K. Prud'homme, I. A. Aksay, and R. Car, *Nano Lett.*, 2008, **8**, 36–41.
41. R. Rao, D. Tishler, J. Katoch, and M. Ishigami, *Phys. Rev. B*, 2011, **84**, 113406.
42. A. Ferrari and J. Robertson, *Phys. Rev. B*, 2000, **61**, 14095–14107.
43. F. Tuinstra, *J. Chem. Phys.*, 1970, **53**, 1126.
44. I. K. Moon, J. Lee, R. S. Ruoff, and H. Lee, *Nat. Commun.*, 2010, **1**, 73.
45. S. Eigler, C. Dotzer, and A. Hirsch, *Carbon N. Y.*, 2012, **50**, 3666–3673.
46. I. Jung, J.-S. Rhyee, J. Y. Son, R. S. Ruoff, and K.-Y. Rhee, *Nanotechnology*, 2012, **23**, 025708.
47. D. L. Duong, G. H. Han, S. M. Lee, F. Gunes, E. S. Kim, S. T. Kim, H. Kim, Q. H. Ta, K. P. So, S. J. Yoon, S. J. Chae, Y. W. Jo, M. H. Park, S. H. Chae, S. C. Lim, J. Y. Choi, and Y. H. Lee, *Nature*, 2012, **490**, 235–9.
48. M. Haïdopoulos, S. Turgeon, G. Laroche, and D. Mantovani, *Plasma Process. Polym.*, 2005, **2**, 424–440.
49. A. Lerf, H. He, M. Forster, and J. Klinowski, *J. Phys. Chem. B*, 1998, **102**, 4477–4482.
50. D. W. Boukhvalov and M. I. Katsnelson, *J. Am. Chem. Soc.*, 2008, **130**, 10697–701.
51. R. John, A. Ashokreddy, C. Vijayan, and T. Pradeep, *Nanotechnology*, 2011, **22**, 165701.
52. J.-T. Chi, H. Y. Chang, G. Haraldsen, F. L. Jahnsen, O. G. Troyanskaya, D. S. Chang, Z. Wang, S. G. Rockson, M. van de Rijn, D. Botstein, and P. O. Brown, *Proc. Natl. Acad. Sci. U. S. A.*, 2003, **100**, 10623–8.
53. A. Schreer, C. Tinson, J. P. Sherry, and K. Schirmer, *Anal. Biochem.*, 2005, **344**, 76–85.